AGU PUBLICATIONS

Geophysical Research Letters

RESEARCH LETTER
10.1002/2014GL061555

Key Points:
- Near-bottom AUV surveys of detachment faulting at Mid-Atlantic Ridge
- Sediment distribution distinguishes active from non-active faults
- Variation in timing of slip quantified between two surveys

Supporting Information:
- Readme
- Figure S1

Correspondence to:
R. Parnell-Turner,
rep52@cam.ac.uk

Citation:
Parnell-Turner, R., J. R. Cann, D. K. Smith, H. Schouten, D. Yoerger, C. Palmiotto, A. Zheleznov, and H. Bai (2014), Sedimentation rates test models of oceanic detachment faulting, *Geophys. Res. Lett.*, *41*, 7080–7088, doi:10.1002/2014GL061555.

Received 15 AUG 2014
Accepted 1 OCT 2014
Accepted article online 2 OCT 2014
Published online 23 OCT 2014

Sedimentation rates test models of oceanic detachment faulting

Ross Parnell-Turner[1], Johnson R. Cann[2], Deborah K. Smith[3], Hans Schouten[3], Dana Yoerger[3], Camilla Palmiotto[4], Alexei Zheleznov[5], and Hailong Bai[6]

[1]Department of Earth Sciences, University of Cambridge, Cambridge, UK, [2]School of Earth and Environment, University of Leeds, Leeds, UK, [3]Woods Hole Oceanographic Institution, Woods Hole, Massachusetts, USA, [4]Istituto di Scienze Marine, CNR, Bologna, Italy, [5]Institute of Earth Sciences, Saint Petersburg State University, St. Petersburg, Russia, [6]Department of Geology, University of Maryland, College Park, Maryland, USA

Abstract Long-lived detachment faults play an important role in the construction of new oceanic crust at slow-spreading mid-oceanic ridges. Although the corrugated surfaces of exposed low-angle faults demonstrate past slip, it is difficult to determine whether a given fault is currently active. If inactive, it is unclear when slip ceased. This judgment is crucial for tectonic reconstructions where detachment faults are present, and for models of plate spreading. We quantify variation in sediment thickness over two corrugated surfaces near 16.5°N at the Mid-Atlantic Ridge using near-bottom Compressed High Intensity Radar Pulse (CHIRP) data. We show that the distribution of sediment and tectonic features at one detachment fault is consistent with slip occurring today. In contrast, another corrugated surface 20 km to the south shows a sediment distribution suggesting that slip ceased ~150,000 years ago. Data presented here provide new evidence for active detachment faulting, and suggest along-axis variations in fault activity occur over tens of kilometers.

1. Introduction

It is now recognized that detachment faulting, leading to the formation of oceanic core complexes, plays a significant role in crustal construction at slow- and ultraslow-spreading ridges [*Tucholke et al.*, 1998; *Smith et al.*, 2006; *Ildefonse et al.*, 2007]. Typically, normal faults accommodate plate spreading through a few hundreds of meters of slip, before becoming inactive as a new generation of normal faults initiates closer to the axis. Slip on detachment faults, by contrast, can lead to heaves (i.e., horizontal displacements) of up to 100 km, exhuming lower crust and upper mantle rocks to the seafloor [*Tucholke and Lin*, 1994; *Cann et al.*, 1997; *Cannat et al.*, 2006; *Smith et al.*, 2006; *Okino et al.*, 2004; *Baines et al.*, 2008; *Grimes et al.*, 2008; *Dick et al.*, 2008].

Corrugations oriented parallel to the direction of spreading have been frequently observed over the surfaces of oceanic detachment faults [*Tucholke and Lin*, 1994; *Cann et al.*, 1997; *Tucholke et al.*, 1998]. Corrugated surfaces are interpreted as the exposed footwall of low-angle detachments, emerging from beneath the hanging wall of the median valley floor [*Cann et al.*, 1997; *Tucholke et al.*, 1998; *MacLeod et al.*, 2002]. Despite the growing evidence that detachment faulting is very common at slow-spreading ridges, only one such area has been studied to determine whether it was actively slipping at depth. A section of the TAG detachment at 26°N on the MAR was the site of a successful seismicity and seismic structure study [*DeMartin et al.*, 2007]. The experiment showed an active dome-shaped fault surface extending between 3 and 7 km below the seafloor. In the absence of these data at other sites, it has been difficult to obtain direct evidence whether a detachment fault in the rift valley wall is active or not. If no longer active, the timing of when a fault stopped slipping is central to understanding the formation and evolution of detachment faulting.

The large number of hydroacoustically detected earthquakes (magnitude of completeness >3; *Bohnenstiehl et al.* [2002]) and a preliminary bathymetric survey provided early clues that detachment faulting plays a major role in crustal accretion in the 16.5°N region of the Mid-Atlantic Ridge [*Smith et al.*, 2008; *Escartín et al.*, 2008]. In 2013, this area was the focus of RV *Knorr* cruise KN210-05 [Figure 1; *Smith et al.*, 2013; *Dick et al.*, 2013]. Here, we use Compressed High Intensity Radar Pulse (CHIRP) data collected using the autonomous underwater vehicle (AUV) *Sentry* during cruise KN210-5 to provide insight into the activity and timing of two detachment faults on the west flank of the axis. In addition to AUV *Sentry* surveys, an extensive program of rock dredging and nine underwater camera (*TowCam*) tows were carried out in the area. These

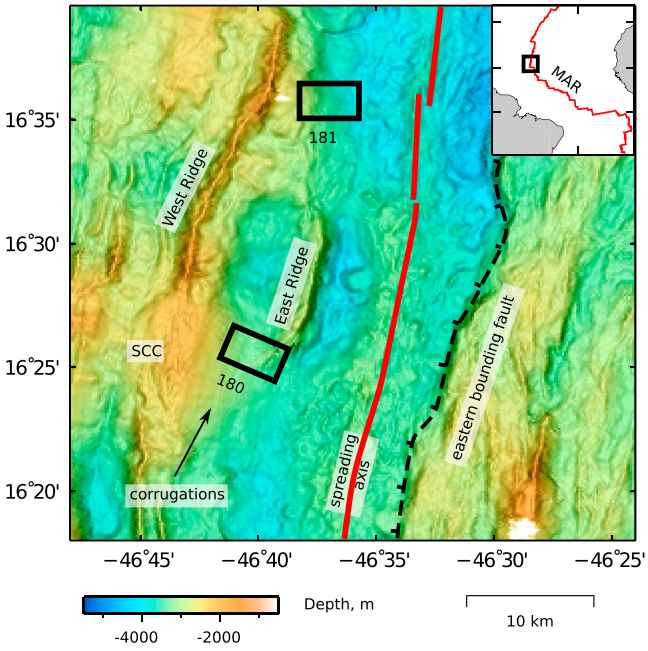

Figure 1. Location map (inset) and multibeam bathymetric map of study area [Cruise KN210-05; *Smith et al.*, 2013]. Numbered black boxes = location of *Sentry* dives 180 and 181; red line = spreading axis; dashed line with tick marks = eastern bounding fault; SCC = South Core Complex.

additional data provide independent constraints on the rock types, sediment cover, and fault terminations at the seafloor.

2. AUV *Sentry* Data

AUV *Sentry* was used to make 14 detailed survey dives within the 16.5°N region. We examine the multibeam bathymetry, side scan sonar and CHIRP data from two of these *Sentry* dives. Each dive covered an area of ~10 km^2. AUV *Sentry* flew at a height of ~65 m above the seafloor, at a speed of ~0.8 m s^{-1} (~1.5 kts). Tracks were spaced ~180 m apart to obtain 100% coverage by the 400 kHz Reson 7125 multibeam sonar, which has a spatial resolution of ~0.5 m. CHIRP profiles, which provide cross-sectional images of shallow sediment cover, were acquired with an Edgetech 2200 M unit operating with a frequency sweep of 4–24 kHz. Vertical resolution is ~10 cm. CHIRP data were processed using open

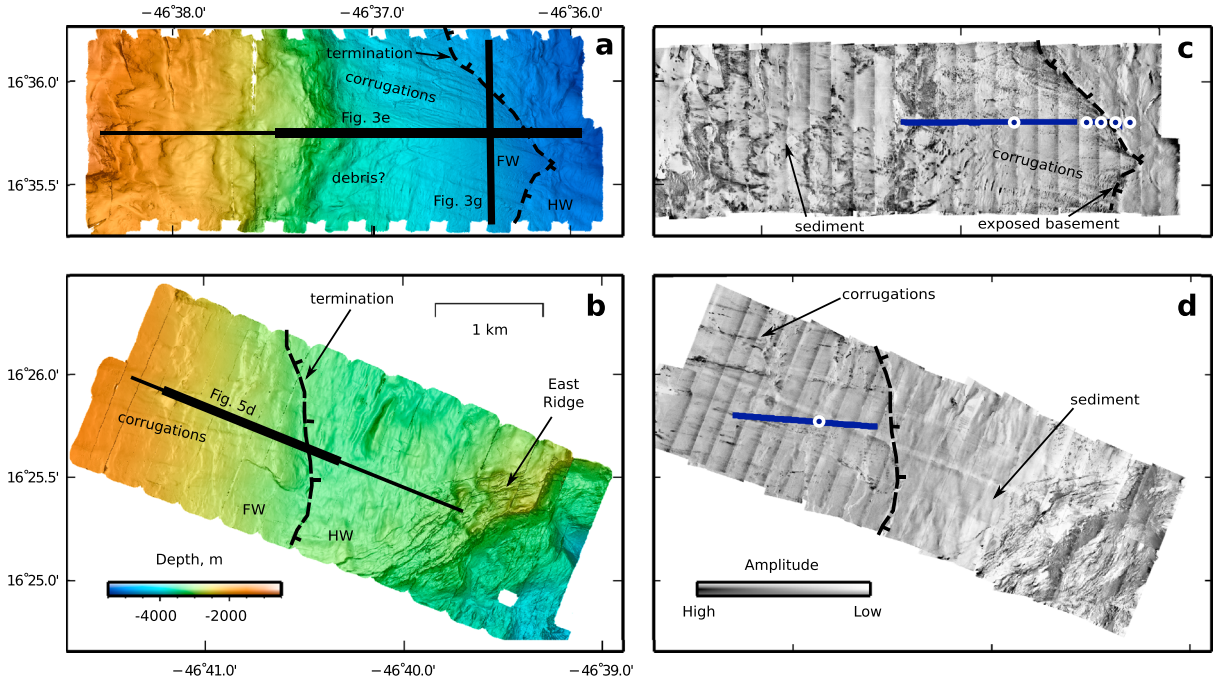

Figure 2. Bathymetric and side scan sonar data from *Sentry* dives 181 and 180 (location shown in Figure 1). (a) High-resolution bathymetric data acquired during *Sentry* dive 181. Black line = location of Compressed High Intensity Radar Pulse (CHIRP) profile in Figure 3a, thickened portions shown in Figures 3e and 3g; dashed line with tick marks = detachment fault termination; FW = footwall; HW = hanging wall. (b) High-resolution bathymetric data acquired during *Sentry* dive 180. Black line = location of CHIRP profile in Figure 5a, thickened portion shown in Figure 5d. (c) Side scan sonar image from dive 181. Blue line = location of *TowCam* dive TC7; white circles = location of *TowCam* photographs shown in Figures S1c–g. Note definition of detachment fault termination identified by high amplitude returns, and clearly visible corrugations. (d) Side scan sonar image from dive 180. Blue line = location of *TowCam* dive TC6; white circle = location of *TowCam* photograph shown in Figure S1h. Note well-defined corrugations on FW, and low amplitude returns on HW suggesting sedimented seafloor.

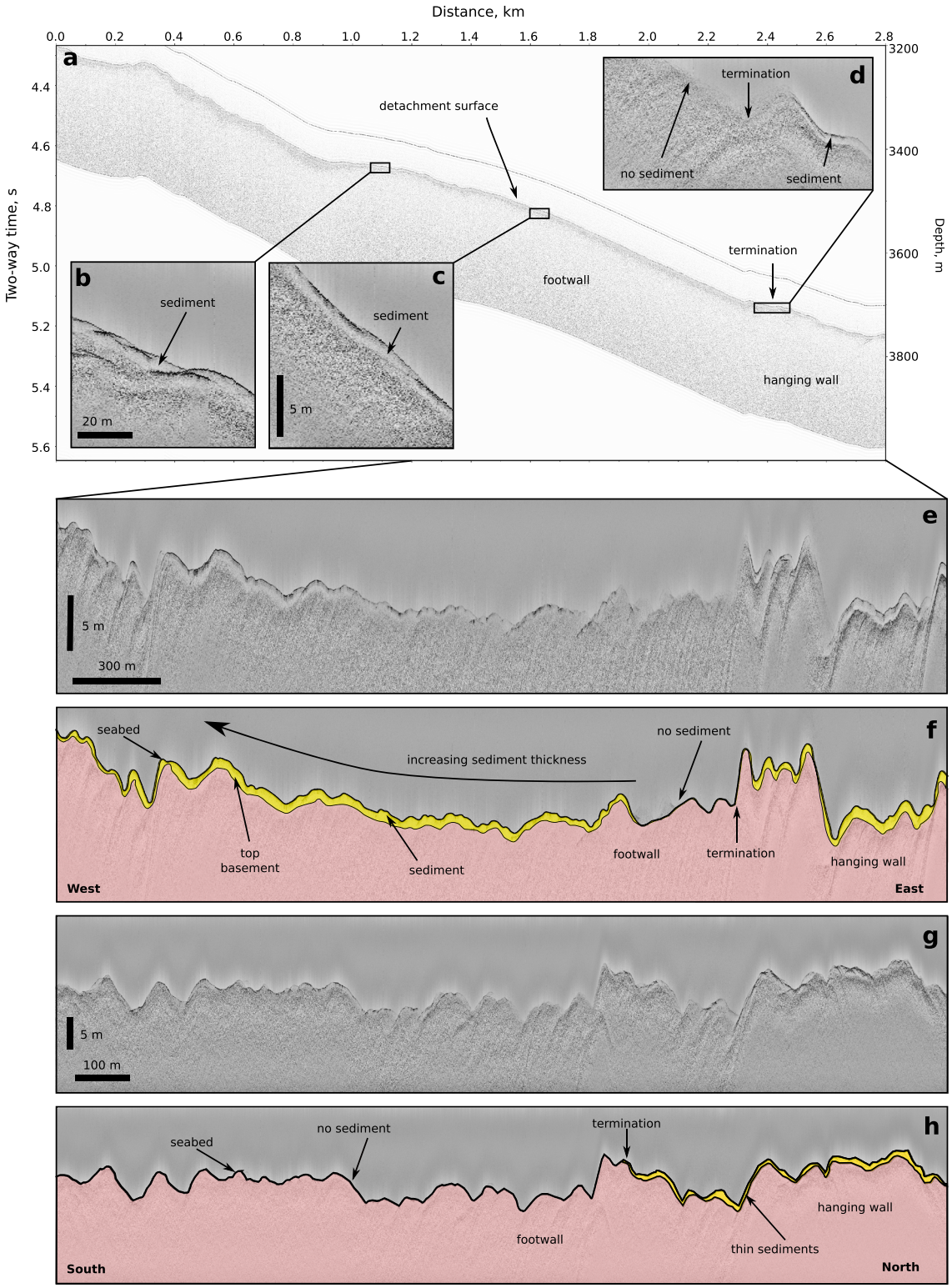

Figure 3

source MB-System and SeismicUnix software packages [*Caress and Chayes*, 1996; *Cohen and Stockwell*, 2013]. Processing consisted of applying a zero-phase, sine-squared bandpass filter (trapezoidal weights 0, 1, 1, 0; frequencies 0.08, 0.1, 24, 25 kHz) to remove noise and frequencies associated with other instruments on the vehicle; static correction according to vehicle depth, and depth conversion using a constant (water) velocity of 1500 m s^{-1}.

3. Sediment Thickness at Two Detachment Faults Near 16.5°N

We compare the results of two *Sentry* dives, 180 and 181, located on the western rift valley wall (Figure 1). Dive 181 was located close to 16° 36′N, ~5.5 km from the crest of the axial volcanic ridge. An evenly dipping (slope ~18°), convex upward, corrugated surface was revealed by the high-resolution bathymetric data. The corrugated surface transitions to an area of irregular topography at the top of the slope (Figure 2a). The fine-scale corrugations on this surface, tens of meters in wavelength, are resolvable only with the high-resolution bathymetric data acquired using *Sentry* [*Smith et al*., 2013]. The corrugations terminate along an arcuate line at the base of the slope, against a terrain that has the hummocky morphology of volcanic seafloor (eastern portion of Figure 2a). In the detachment fault interpretation, this termination would be the line along which the footwall of the detachment emerges at the seafloor from beneath a hanging wall (i.e., the inner valley floor in this case). Approximately 1.5 km to the west of the fault termination, the low-angle corrugated surface appears to be covered by debris, most likely to be material eroded from upslope.

High amplitude (i.e., dark) returns from the tops of the corrugations near the termination in the side scan sonar image suggest basement rock protruding from beneath a thin covering of sediment (Figure 2c). The termination itself is sharp in character. Immediately to the west of the termination, sonar returns from the most recently exposed footwall are high in amplitude, indicating outcropping basement or very thin sediment cover.

Figure 3 shows a CHIRP profile crossing the termination of the corrugated surface from dive 181. Sediments are 1–2 m thick on the upper slopes of the domed detachment surface (footwall, Figure 3b), and progressively thin downslope (Figure 3c). No resolvable sediment is observed near the western side of the termination (Figure 3d). Sediment thickness maps were constructed from the CHIRP profiles collected along the *Sentry* tracklines. Profiles are spaced 180 m apart and run across the survey; a single profile was collected through the middle of each survey (black lines, Figures 2a and 2b). Seabed and sediment-basement reflections were hand-picked along flattened CHIRP profiles, and converted from two-way travel time to depth using a constant (water) velocity of 1500 m s^{-1}. These horizons were used to create a gridded isopach of sediment thickness for each dive area. The resulting map shows varying amounts of sediment cover, decreasing downslope toward the termination (Figure 4a). Profiles closest to the termination are devoid of resolvable sediment. The lack of sediment adjacent to the termination implies that slip is currently occurring on the detachment fault at dive 181. Patches of thicker sediment close to the top of the footwall slope in Figure 4a are likely to be the result of material slumped from higher up. In general, to the east of the termination on the hanging wall side, sediment is ~2 m thick (Figures 3d, 3e, and 3f). Profiles oriented perpendicular to the slip direction on the hanging wall side also show a sediment thickness of ~2 m (Figures 3g and 3h).

The discontinuity in sediment thickness is confirmed by photographs acquired at the seafloor during deep-towed imaging surveys with the *TowCam* imaging system [*Fornari*, 2003]. Seafloor photographs acquired at dives 180 and 181 are presented in the supporting information (location shown in Figure 2;

Figure 3. CHIRP profiles acquired during *Sentry* dive 181 (see Figure 2a for location). Insets (b)–(d) plotted at same scale. (a) Profile extending west–east through the center of the survey across the detachment surface. (b) Detailed inset showing ~1–2 m thick sediment cover on upper (west) slope of detachment surface. (c) Detailed inset showing sediment progressively thinning downslope. (d) Detailed inset at the detachment termination, showing absence of sediment west of the termination (footwall), and 1 m of sediment immediately east on the hanging wall. (e) Detailed portion of profile in Figure 3a, flattened according to height of *Sentry* vehicle above the seafloor to remove the effect of steep bathymetric slopes to aid interpretation seafloor (see Figure 2a for location). Note variation in sediment thickness across the detachment surface. (f) Interpreted version of Figure 3e, note location of termination and increasing up-slope sediment cover. Yellow shading: sediment; pink shading: basement. (g) Profile oriented perpendicular to footwall corrugations, flattened according to height of *Sentry* vehicle above the seafloor (location shown in Figure 2a). (h) Interpreted version of Figure 3g. Note lack of sediment south of the termination, and consistent veneer of sediment on the hanging wall side of profile.

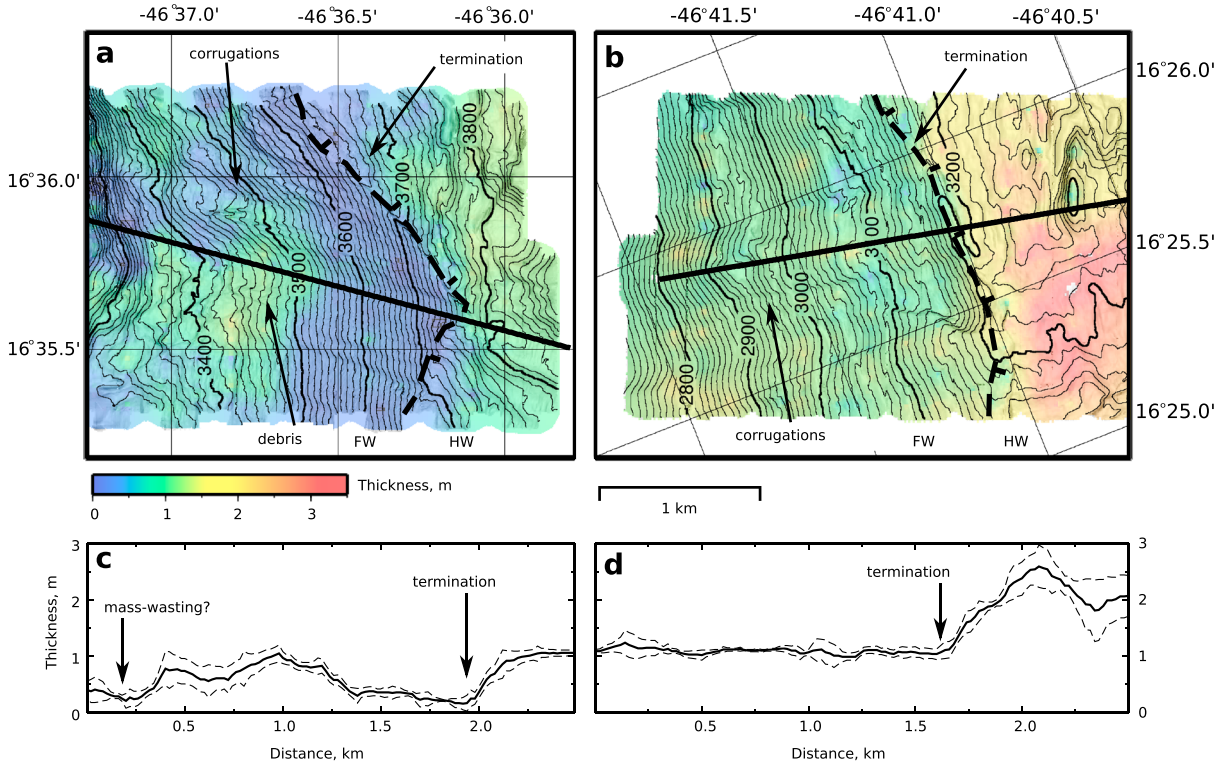

Figure 4. Sediment thickness maps, calculated from interpreted CHIRP profiles and gridded at 25 m resolution. Bathymetric contours with depths labeled in meters; dashed black lines with tick marks = detachment fault terminations; solid black lines = location of sediment thickness profiles in Figures 4c and 4d. (a) Dive 181. Sediment is <1 m thick to west of termination on footwall (FW), suggesting fault is active today. Sediment is 1–2 m thick on hanging wall (HW) side of termination. Note thickened sediment at center of corrugated surface, perhaps due to local slumping. Dashed line with tick marks = fault termination. (b) Dive 180 (oblique Mercator projection). Sediment is ~1 m thick adjacent to termination on FW; thickens to ~1.5 m westward upslope. Sediment on HW side is 2–3 m thick. (c) Sediment thickness profile, dive 181. Thin black line with dashed band = mean sediment thickness ±1 standard deviation. Note possible mass wasting at western end of profile, which causes sediment thickness to diminish. (d) Sediment thickness profile, dive 180.

photographs in Figure S1). Figure S1c shows that in the area covered by dive 181, sediment blankets the western part of the corrugated surface, far from the termination. About 150 m west of the termination, the detachment surface is partly sediment covered with numerous rock fragments (Figure S1d). The approach to the termination is shown in Figure S1e, where a very thin sediment layer partly covers the basement. The ~10 m high edge of the hanging wall at the termination (with overlying sediments) is imaged in Figure S1f. The sediment covered hanging wall is shown in Figure S1g.

Dive 180 was located ~20 km south of dive 181. It is ~10 km from the volcanic axis and covers the northern section of the corrugated surface of South Core Complex (SCC; Figure 1). Between the eastern extent of the corrugated surface of the SCC in dive 180 and the volcanic spreading axis is a more recent normal fault, called East Ridge. This fault is the new inner valley floor boundary fault. Assuming that East Ridge fault initiated 3.5 km from the axis, it has been active for ~200 ka [*Smith et al.*, 2008]. *Smith et al.* [2013] suggested that the section of the SCC detachment fault behind East Ridge stopped slipping when East Ridge fault formed. Dive 180 examined this section of the SCC fault and its possible extinct termination.

Bathymetric data from dive 180 show the corrugated surface to be a uniformly convex surface terminating at a break in slope against the fill of the basin behind East Ridge (Figure 2c). The termination of the fault with the basin material is sharp and easily identified. High amplitude returns on side scan images reveal a pattern of parallel corrugations to the west of the fault termination (Figure 2d). A CHIRP profile oriented roughly parallel to the corrugations and straddling the termination is shown in Figure 5. Sediment of variable thickness blankets the entire survey area, including a 0.5–2 m thick veneer of sediment over the domed corrugated surface (Figures 4b and 5). *TowCam* images show that sediment blankets the seafloor to the west

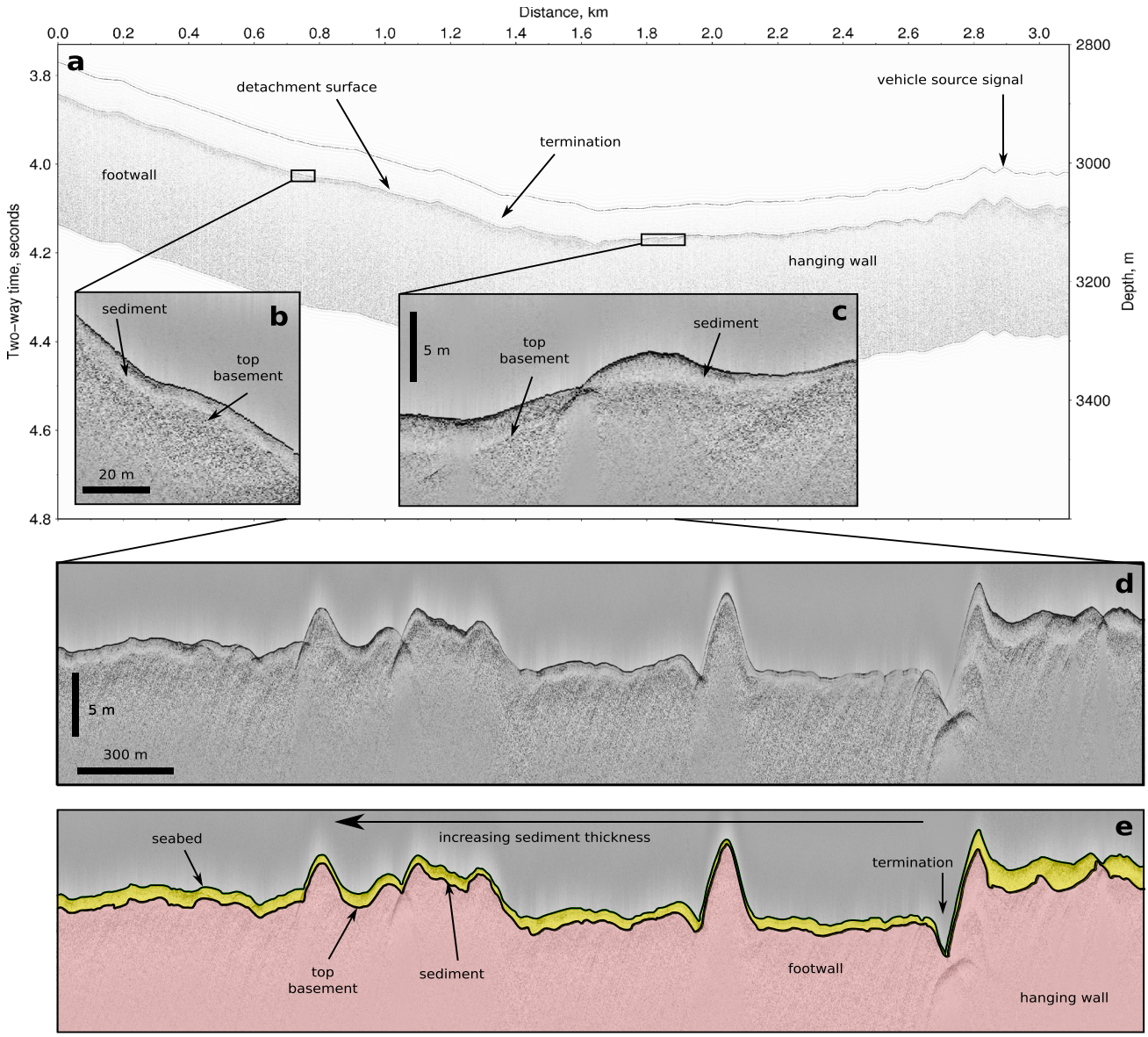

Figure 5. CHIRP profile acquired during *Sentry* dive 180 (see Figure 2b for location). Insets (b) and (c) plotted at same scale. (a) Profile extending west–east through the center of the survey across detachment surface. (b) Detailed inset showing ~1–2 m thick sediment cover on footwall of domed detachment surface. (c) Detailed inset showing ~2 m thick sediment on hanging wall. (d) Detailed portion of profile in Figure 5a, flattened according to height of *Sentry* vehicle above the seafloor (see Figure 2b for location). Note sediment is present in both hanging wall and footwall sides of termination. (e) Interpreted version of Figure 5d, note location of termination and increasing sediment thickness westward. Yellow shading: sediment; pink shading: basement.

(i.e., footwall side) of the termination (Figure S1h). The presence of sediment adjacent to the termination on the footwall is in contrast with dive 181, where no resolvable sediment on the footwall close to the termination is observed. This observation suggests that the section of SCC detachment fault imaged during dive 180 is not actively slipping. In common with the sediment thickness variations at dive 181, there is a sharp break in sediment thickness across the termination (Figures 5d and 5e). Sediment is about 2 m thick on the hanging wall east of the termination, and $<$ ~1 m thick on the footwall immediately to the west of the termination. CHIRP profiles oriented perpendicular to the corrugations also show this sharp contrast in sediment thickness either side of the termination (Figure 4b). As in the results from dive 181, sediment thickness increases westward (i.e., upslope) along the footwall, from ~1 m adjacent to the termination up to ~1.5–2 m at the top of the slope. Our data do not indicate any obvious mass wasting of the detachment footwall at dive 180.

4. Discussion

In a simple interpretation of detachment faulting, the footwall at the termination should be the most recent section exhumed to the seafloor, and the time of exposure of the footwall should increase with distance from the termination. Thus, in an active detachment, the footwall near the termination should be more recently exposed than at an inactive detachment. We test and develop this hypothesis below.

Combining observations from AUV *Sentry* bathymetric data, side scan sonar images, CHIRP profiles, and *TowCam* seafloor photographs has allowed us to locate the terminations of two detachment faults in the western rift valley wall in the 16.5°N region (dives 181 and 180; Figure 1). At both terminations the sediment thickness shows a sharp increase from the corrugated footwall onto the un-corrugated hanging wall, and a gradual increase in thickness away from the termination westward across the corrugated footwall. This is consistent with the simple interpretation above.

At dive 181, the 0–0.5 m thick sediment on the corrugated surface immediately adjacent to the termination suggests that it is actively emerging at the seafloor. There has not been enough time for significant sediment to accumulate. The observed upslope thickening of sediments is consistent with the increase in time that the footwall has been exposed at the seafloor. In dive 180 by contrast, the 1 m thick sediment cover on the footwall adjacent to the termination suggests that the detachment fault there is not active today and has been inactive for long enough for 1 m of sediment to accumulate. Here again, the sediment thickens westward away from the termination consistent with past slip on the detachment, and an increase in length of time the footwall has been exposed at the seafloor. These observations also are consistent with our initial simple interpretation of fault behavior.

We use two independent estimates of sedimentation rate to quantify the timing and rate of slip on the SCC and dive 181 detachment faults. First, constraints on the lithology and accumulation rate of sediments in the region can be obtained from sediment cores recovered nearby. The nearest sediment sample was collected ~75 km north of our study area in a piston core at site V23-112 (17°16′N, 46°45′W; 2845 m water depth). Sediments at this site consist of foraminiferal ooze, greyish-orange in color, with a very high carbonate content [*National Geophysical Data Center digital archive*], in good agreement with sediments recovered during our dredge hauls in the 16.5°N study area. The sediment accumulation rate calculated from V23-112 and one other nearby piston core recovered nearest to the ridge axis in this region is 7 ± 2 mm ka^{-1} [*Damuth*, 1977]. Second, we use the half-spreading rate at 16.5°N as an alternative approach to estimate the sedimentation rate, as follows. If we assume that slip on a detachment fault accounts for half of the extension at a spreading center the slip on the faults would be at the half-spreading rate of 12.5 mm a^{-1} [*Fujiwara et al.*, 2003], implying that the 1.5 km long corrugated surface at dive 181 took ~120 ka to form. The observed 1 m thick sediment located at the top of this corrugated surface, 1.5 km west of the termination, must have accumulated over this ~120 ka period, yielding a sedimentation rate of 8 mm ka^{-1}. Combining these two independent estimates gives a mean sedimentation rate of ~7 ± 2 mm ka^{-1}.

We use this accumulation rate to quantify the time at which slip ceased on the fault at dive 180. Since we observe on average, 1 m of sediment adjacent to the termination at dive 180, slip on that fault must have ceased at 150 ± 50 ka. This timing is consistent with the structural estimate that slip began on East Ridge at approximately 200 ka [*Smith et al.*, 2008], suggesting that when East Ridge fault formed, the detachment at dive 180 ceased extending. Finally, the 2 m thick sediment on the hanging wall side of the terminations at both dive 180 and 181 implies that the hanging walls have not been volcanically resurfaced for ~300 ± 100 ka.

Observations of continental detachment faults suggest that cataclasites and fault breccias are thickest on the lateral walls of fault corrugations [*John*, 1987; *Davis and Lister*, 1988]. Sediments might also be expected to accumulate in the troughs of corrugations [*Davis et al.*, 1993]. Our observations show that perpendicular to the spreading direction, corrugations are more or less uniformly covered in sediment at the resolution of the CHIRP data (cms). Toward the lower slopes of the detachment surface at dive 181, the corrugations appear to be sediment-free (see corrugation-perpendicular CHIRP profile in Figure 3g). The possible effects of mass wasting upon the distribution of sediment across the study area also should be considered. Headwall scars on the upper slopes of the 181 detachment fault (Figure 1b), and irregular variations in sediment thickness (Figures 3, 4, and 5), suggest that mass wasting plays a role in redistributing sediment here. Sediment is likely to be slumping eastward off the upper slope in the dive 181 area, but it does not appear to be accumulating near the termination (Figures 2e and 2f). Nonetheless, sediment redistribution through land

sliding as well as ocean currents may explain the uneven and occasionally patchy sediment at the top of the detachment footwall slopes. Turbulent oceanic mixing and stronger tidal currents are more likely in locations of rough bathymetry [*Ledwell et al.*, 2000], such as on the uneven terrain on the upper slopes of detachment fault surfaces (Figures 2 and 4).

5. Conclusions

We have presented observations of sediment thickness over oceanic detachment faults using near-bottom CHIRP data acquired by AUV *Sentry*. Overall the distribution of sediment thicknesses is consistent with a simple interpretation of detachment faulting. In this hypothesis, a corrugated surface emerges from beneath the hanging wall at the fault termination, then spreads steadily away from the termination and the volcanic axis. The low-angle, corrugated detachment fault imaged with dive 181 has a sharp termination located 4.5 km from the axis. The footwall, where it emerges from beneath the valley floor, has 0–0.5 m thick sediment cover. These observations suggest that this surface is recently exposed at the surface and thus is actively slipping today. A section of the low-angle, corrugated SCC detachment (dive 180) located ~20 km to the south of dive 181, and ~10 km from the volcanic axis also has a sharp termination. Near to the termination the exposed surface has ~1 m of sediment. Assuming a sedimentation rate of 7 ± 2 mm ka^{-1}, this part of the SCC detachment fault has been inactive for 150 ± 50 ka, which is consistent with slip initiating closer to the axis on East Ridge fault at ~200 ka [*Smith et al.*, 2008]. Our results suggest that the style of active normal faulting in this region varies along axis on scales as short as 20 km. Determinations of sediment thickness from near-bottom CHIRP data have allowed us to make a significant step forward in quantitatively unraveling the tectonic history of an area dominated by detachment faulting.

Acknowledgments

Data are available upon request from the author. This work was supported by the National Science Foundation grant number OCE-1155650. We thank the Captain and crew of RV *Knorr* for their excellent support and dedication during Cruise KN210-05. We are also grateful to the *Sentry* group and to the entire scientific party. We thank M. H. Cormier and N. Hayman for constructive reviews. Earth Sciences contribution esc.3135.

Eric Calais thanks Marie-Helene Cormier and Nicholas Hayman for their assistance in evaluating this manuscript.

References

Baines, A. G., M. J. Cheadle, B. E. John, and J. J. Schwartz (2008), The rate of oceanic detachment faulting at Atlantis Bank SW Indian Ridge, *Earth Planet. Sci. Lett.*, *273*, 105–114.

Bohnenstiehl, D. R., M. Tolstoy, R. P. Dziak, C. G. Fox, and D. K. Smith (2002), Aftershock sequences in the mid-ocean ridge environment: An analysis using hydroacoustic data, *Tectonophysics*, *354*(1–2), 49–70.

Cann, J. R., D. K. Blackman, D. K. Smith, E. McAllister, B. Janssen, S. Mello, E. Avgerinos, A. R. Pascoe, and J. Escartín (1997), Corrugated slip surfaces formed at North Atlantic ridge-transform intersections, *Nature*, *385*, 329–332.

Cannat, M., D. Sauter, V. Mendel, E. Ruellan, K. Okino, J. Escartín, V. Combier, and M. Baala (2006), Modes of seafloor generation at a melt-poor ultraslow-spreading ridge, *Geology*, *34*, 605–608.

Caress, D. W., and D. L. Chayes (1996), Improved Processing of Hydrosweep DS Multibeam Data on the R/V Maurice Ewing, *Mar. Geophys. Res.*, *18*, 631–650.

Cohen, J. K., and J. W. Stockwell (2013), CWP/SU: Seismic Un*x. Release No. 43R5: An open source software package for seismic research and processing, Center for Wave Phenomena, Colo. School of Mines, Golden, Colo.

Damuth, J. E. (1977), Late Quaternary sedimentation in the western equatorial Atlantic Late Quaternary sedimentation in the western equatorial Atlantic, *Geol. Soc. Am. Bull.*, *88*, 695–710.

Davis, G. A., and G. S. Lister (1988), Detachment faulting in continental extension; Perspectives from the Southwestern U.S. Cordillera, *Geol. Soc. Am. Spec. Pap.*, *218*, 133–159.

Davis, G. A., T. K. Fowler, K. M. Bishop, T. C. Brudos, S. J. Friedmann, D. W. Burbank, M. A. Parke, and B. C. Burchfiel (1993), Pluton pinning of an active Miocene detachment fault system, eastern Mojave Desert, California, *Geology*, *21*(7), 627.

DeMartin, B. J., R. A. Sohn, J. P. Canales, and S. E. Humphris (2007), Kinematics and geometry of active detachment faulting beneath the Trans-Atlantic Geotraverse (TAG) hydrothermal field on the Mid-Atlantic Ridge, *Geology*, *35*(8), 711–714.

Dick, H. J. B., M. A. Tivey, and B. E. Tucholke (2008), Plutonic foundation of a slow-spreading ridge segment: Oceanic core complex at Kane Megamullion, 23°30′N, 45°20′W, *Geochem. Geophys. Geosyst.*, *9*, Q05014, doi:10.1029/2007GC001645.

Dick, H. J. B., D. K. Smith, J. R. Cann, H. Schouten, H. Marschall, R. E. Parnell-Turner, and D. Yoerger (2013), Crustal Heterogeneity and Stratigraphy on the Mid-Atlantic Ridge at 16°-17°N, Abstract OS41E-06 presented at 2013 Fall Meeting, AGU, San Francisco, Calif., 9–13 Dec.

Escartín, J., D. K. Smith, J. R. Cann, H. Schouten, C. H. Langmuir, and S. Escrig (2008), Central role of detachment faults in accretion of slow-spreading oceanic lithosphere, *Nature*, *455*(7214), 790–4.

Fornari, D. J. (2003), A new deep-sea towed digital camera and multi-rock coring system, *Eos Trans. AGU*, *84*, 69–76, doi:10.1029/2003EO080001.

Fujiwara, T., J. Lin, T. Matsumoto, P. B. Kelemen, B. E. Tucholke, and J. F. Casey (2003), Crustal evolution of the Mid-Atlantic Ridge near the Fifteen-Twenty Fracture Zone in the last 5 Ma, *Geochem. Geophys. Geosyst.*, *4*, 1024, doi:10.1029/2002GC000364.

Grimes, C. B., B. E. John, M. J. Cheadle, and J. L. Wooden (2008), Protracted construction of gabbroic crust at a slow spreading ridge: Constraints from 206 Pb/ 238 U zircon ages from Atlantis Massif and IODP Hole U1309D (30°N, MAR), *Geochem. Geophys. Geosyst*, *9*, Q08012, doi:10.1029/2008GC002063.

Ildefonse, B., D. K. Blackman, B. E. John, Y. Ohara, D. J. Miller, and C. J. MacLeod (2007), Oceanic core complexes and crustal accretion at slow-spreading ridges, *Geology*, *35*(7), 623–626.

John, B. E. (1987), Geometry and evolution of a mid-crustal extensional fault system: Chemehuevi Mountains, southeastern California, in *Continental Extensional Tectonics*, edited by M. P. Coward, J. F. Dewey, and P. L. Hancock, pp. 313–335, *Geol. Soc.*, London, U. K.

Ledwell, J. R., E. T. Montgomery, K. L. Polzin, L. C. St. Laurent, R. W. Schmitt, and J. M. Toole (2000), Evidence for enhanced mixing over rough topography in the abyssal ocean, *Nature*, *403*, 179–82.

MacLeod, C. J., et al. (2002), Direct geological evidence for oceanic detachment faulting: The Mid-Atlantic Ridge, 15 45′ N, *Geology*, *30*(10), 879–882.

Okino, K., K. Matsuda, D. M. Christie, Y. Nogi, and K. Koizumi (2004), Development of oceanic detachment and asymmetric spreading at the Australian-Antarctic Discordance, *Geochem. Geophys. Geosyst.*, *5*, Q12012, doi:10.1029/2004GC000793.

Smith, D. K., J. R. Cann, and J. Escartín (2006), Widespread active detachment faulting and core complex formation near 13°N on the Mid-Atlantic, *Nature*, *442*, 440–443.

Smith, D. K., J. Escartín, H. Schouten, and J. R. Cann (2008), Fault rotation and core complex formation: Significant processes in seafloor formation at slow-spreading mid-ocean ridges (Mid-Atlantic Ridge, 13°–15°N), *Geochem. Geophys. Geosyst.*, *9*, Q03003, doi:10.1029/2007GC001699.

Smith, D. K., H. Schouten, H. J. B. Dick, and J. R. Cann (2013), Development of different modes of detachment faulting at intermediate magma supply, Abstract T23F-2657 presented at 2013 Fall Meeting, AGU, San Francisco, Calif., 5–9 Dec.

Tucholke, B. E., and J. Lin (1994), A geological model for the structure of ridge segments in slow spreading ocean crust, *J. Geophys. Res.*, *99*, 11,911–937,958.

Tucholke, B. E., J. Lin, and M. C. Kleinrock (1998), Megamullions and mullion structure defining oceanic metamorphic core complexes on the Mid-Atlantic Ridge, *J. Geophys. Res.*, *103*, 9857–9866, doi:10.1029/98JB00167.